Electronic Supplementary Material (ESI) for Physical Chemistry Chemical Physics.

Supporting Information

Extent of Conjugation in Diazonium-Derived Layers in Molecular Junction Devices Determined by Experiment and Modelling

Colin Van Dyck, Adam Johan Bergren, Vineetha Mukundan, Jerry A. Fereiro, and Gino A. DiLabio

A. Optical transitions of *para*-, *meta*- and *ortho*- AB

We report the UV-vis spectrum of the *ortho*-AB 5-mer structure in the main text. We explained that the *ortho* structure led to a splitting of the main π-π* transition. This is evidenced by a direct comparison of the computed spectra of *para*- and *meta*- 5-mer structures, as reported in Figure S1. A *para* connection is dominated by a single transition with a significantly higher oscillator strength. A *meta* connection is dominated by a single transition and a secondary transition that slightly shifts the peak away from the main transition. On the other hand, the *ortho* structure is not dominated by a single transition. The absorption peak is a composite of five significant transitions. This broadens the adsorption spectrum of the *ortho* grown structures.

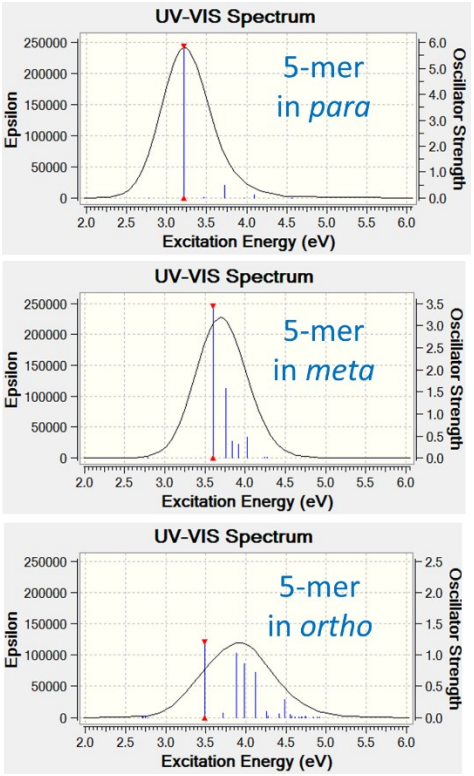

Figure S1. Aligned UV-vis absorption spectra, computed from TD-DFT, for AB 5-mers connected exclusively with *para*, *meta* and *ortho* motifs.

B. Computed Raman spectra of para-, meta- and ortho- AB/NAB

Measured Raman spectra of AB and NAB multilayers, grown using diazonium chemistry, have been reported in past literature. We report those spectra in Figure S2, together with our computed Raman spectra. The Raman calculations are done using the BP86 functional and 6-31G(d,p) basis sets, with unscaled vibrations. This functional is known to predict vibration frequencies with accuracy that is satisfactory [J. Neugebauer and B. A. Hess, The Journal of Chemical Physics, 2003, 118, 7215-7225]. The main conclusion of this comparison is that every connection compares fairly well with the experimental data. On this basis, Raman spectroscopy cannot unambiguously distinguish between *para*, *meta* or *ortho* growth patterns. Moreover, the *ortho* structure we propose in the main manuscript cannot be rejected on the basis of a Raman analysis. In general, each configuration has advantages for a few selected peaks and it cannot be excluded that the grown layers are a mixture of different binding motifs.

Raman spectra calculations of selected structures were performed using the BP86 exchange-correlation functional with 6-31G(d,p) basis sets. Unscaled vibrational frequencies are reported, as this functional is known to predict vibration frequencies with accuracy that is satisfactory for the needs of the present study.[1]

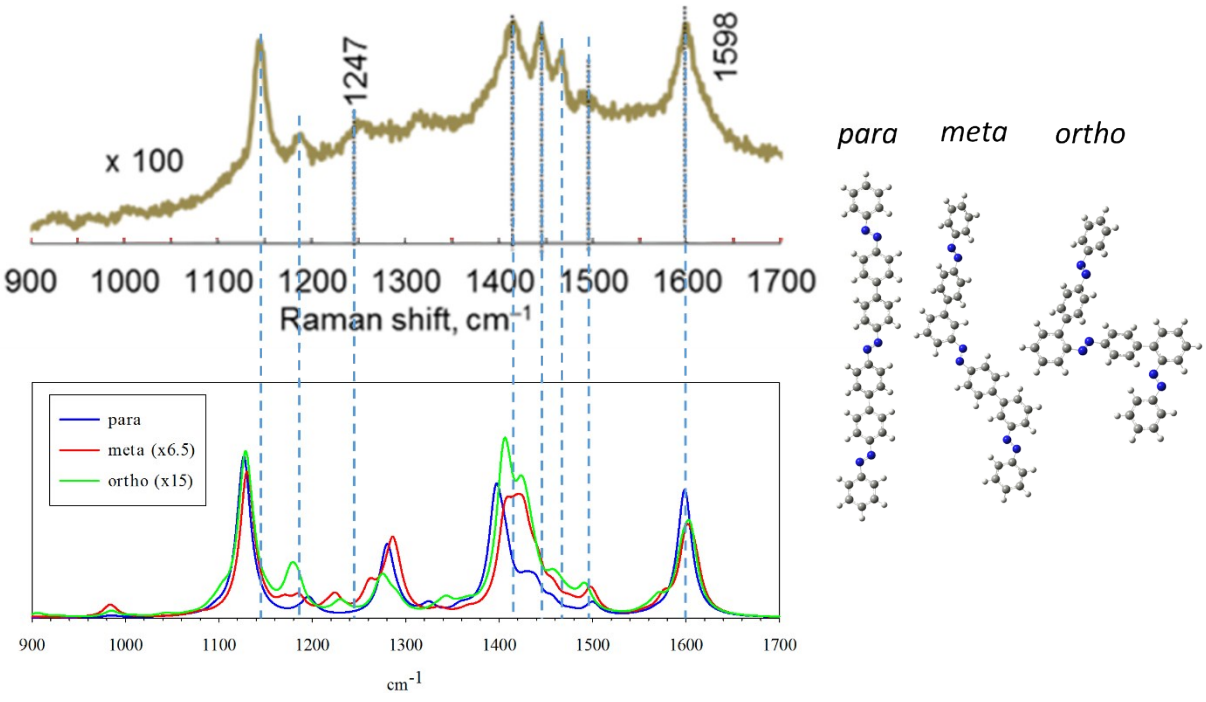

Figure S2. Aligned experimental and simulated AB Raman spectra. Experimental curve is taken from *Supur et al, Anal. Chem. 2017, 89, 6463*. On the right are represented the three structures used in the Raman spectra simulations.

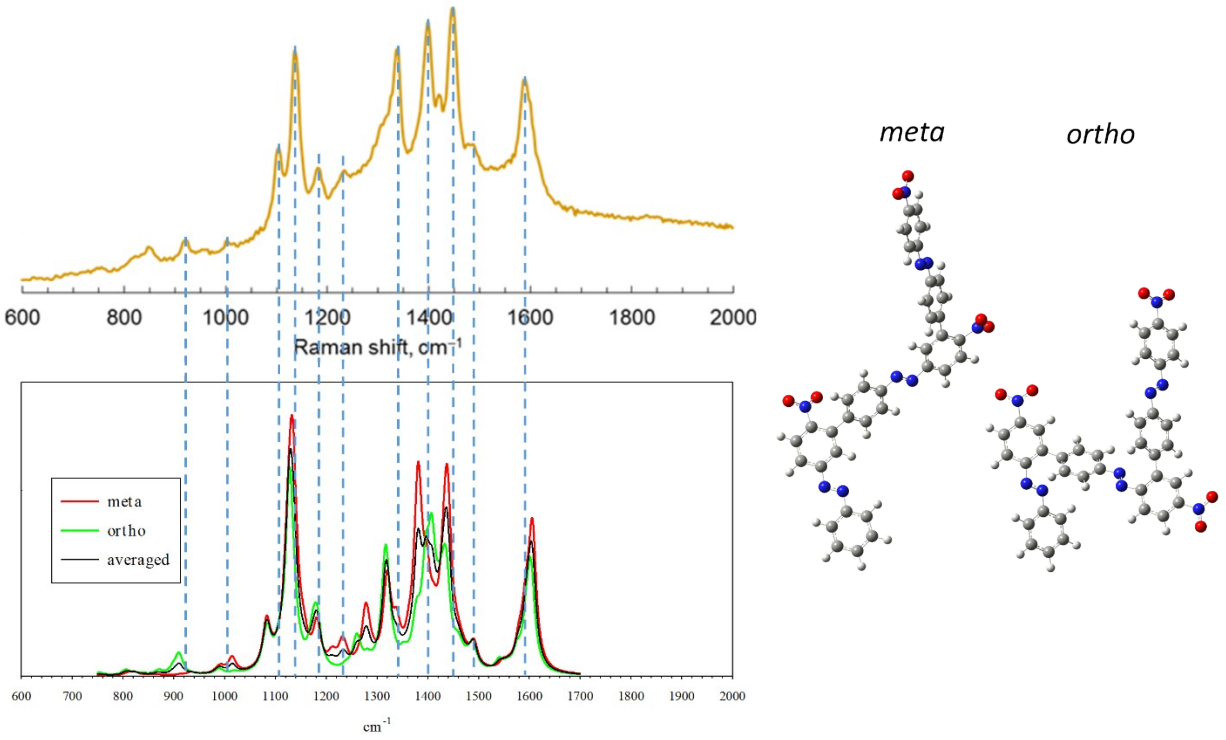

Figure S3. Aligned experimental and simulated NAB Raman spectra. A 50-50 averaging of the *meta* and *ortho* configurations is also reported. Experimental curve is taken from *Supur et al, Anal. Chem. 2017, 89, 6463*. On the right are represented the two structures used in the Raman spectra simulations.

Simulated Raman spectra of grown layers

As a check on the structural features of the nanoscale films grown using the reduction of diazonium reagents, we simulated the Raman spectra of AB and NAB chains and compare these results to previously reported Raman spectra for AB and NAB thin-films[2]. The simulation results for *ortho* and *meta*-linked 3-mers of NAB, their averaged spectrum, and the experimental spectrum are reported in Figure S4.

The overall visual agreement between theory and experiment is reasonable, with all the main experimental features reproduced by the simulations. However, the comparison between the *ortho* and *meta* structures show subtle differences in the position and intensity of specific modes. Similar conclusions apply for the AB structure.

Interestingly, a 50-50 mixing of the *ortho* and *meta* spectra leads to a better comparison between experimental and theoretical spectra. Indeed, the relative intensities of the three main peaks from 1300 to 1500 cm^{-1} compares well with the experimental trend in this scenario. This suggests that a mixture of *ortho* and *meta* connections within the film is plausible.

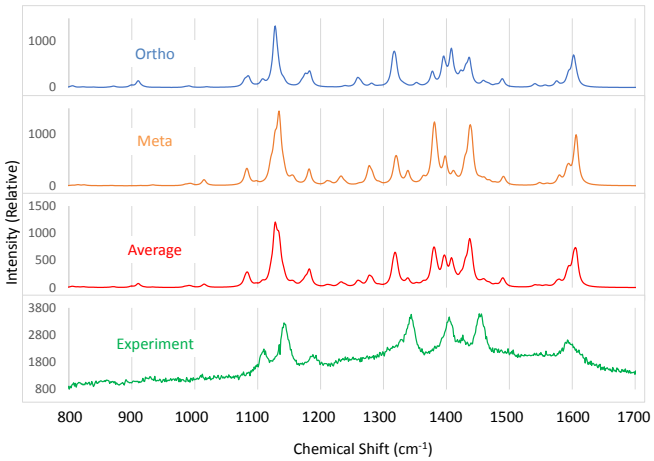

Figure S4. Raman spectra of NAB structures, calculated for all *ortho* and all *meta* 3-mers. The averaged spectrum is also shown, along with the experimental spectrum.

C. Statistical approach and configuration counting

Here we report how we computed the occurring frequencies of each binding motif reported in the main text, with Figure S5 showing the site number scheme.

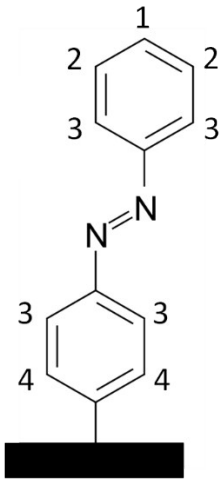

Figure S5. Numbering of the different binding sites.

While we have not carried out an extensive study of how sterics will alter the probability of each type of structure to form, there are several considerations that should be noted. First, the surface of the substrate has sufficient undulations that an initial bonding of the AB unit can lead to a wide variety of orientations. While the localized site is likely to have the AB unit oriented essentially perpendicular to the surface, if this happens on the slope of an undulation, then the sites 2, 3, and 4 can be just as accessible as site 1, or in some geometries, more so. Taking an average across the surface, this can lead to the sites 1-4 being accessible in essentially equal proportion. Second, when there is a single branch point that starts with, for example, a dimer formed from meta- or ortho- bonding (see Figure 2C), the subsequent bonding is more likely to occur at any remaining site because the orientation of the second unit can be such that all sites are more accessible. Third, the original monomer is also available in the case of the branched structure,

which means that not all structures can preclude that two molecules are bonded to the initial monomer. Fourth, if we compare AB and NAB, then the 1 position is precluded for NAB due to the presence of the Nitro group. Thus, we anticipate that there will be a significant difference in behaviour if there is little or no branching. This is in direct contrast with the experimental data in Figure 4 of the main text, where no differences were observed between these two species. Note finally that Table S1 shows that structures that include site 3 motifs (i.e., ortho- linkages) are the most common under the assumption of equal probabilities for each bonding site.

Table S1. List of structure types and probabilities. The overall probability listed in this table is for each *n*-mer. Thus, the total percentages for the 2-mers, 3-mers, and 4-mers will sum to 100%, and there are a total of 9, 68, and 375 structures available, respectively. This is because there is one possible site 1 attachment, two possible sites for type 2 and 4 attachments, and 4 for type 3, making the type 3 motifs the most probably. This analysis assumes equal bonding probability at each site. The most and least probable structures are highlighted using bold text.

2-mer type	Probability (%)		
1	**11.111**		
2	22.222		
3	**44.444**		
4	22.222		
3-mer type	**Probability (%)**	**3-mer type**	**Probability (%)**
1-1	**0.6536**	*2-1*	2.614
1-2	2.614	*2-2*	3.922
1-3	5.229	*2-3*	10.458
1-4	2.614	*2-4*	5.229
3-1	5.229	*4-1*	2.614
3-2	10.458	*4-2*	5.229
3-3	**18.301**	*4-3*	10.458
3-4	10.458	*4-4*	3.922
4-mer type	**Probability (%)**	**4-mer type**	**Probability (%)**
1-1-1	**0.0261**	*1-2-1*	0.2092
1-1-2	0.1569	*1-2-2*	0.5229
1-1-3	0.3137	*1-2-3*	1.2549
1-1-4	0.1569	*1-2-4*	0.6275
1-3-1	0.4183	*1-4-1*	0.2092
1-3-2	1.2549	*1-4-2*	0.6275
1-3-3	2.3007	*1-4-3*	1.2549
1-3-4	1.2549	*1-4-4*	0.5229
2-1-1	0.2092	*2-2-1*	0.4706
2-1-2	0.5229	*2-2-2*	0.6275
2-1-3	1.2549	*2-2-3*	1.8824
2-1-4	0.6275	*2-2-4*	0.9412
2-3-1	1.2549	*2-4-1*	0.6275
2-3-2	2.0915	*2-4-2*	1.4058
2-3-3	**4.6013**	*2-4-3*	2.5098
2-3-4	2.5098	*2-4-4*	1.4058
3-1-1	0.4183	*3-2-1*	1.2549
3-1-2	1.2549	*3-2-2*	2.0915
3-1-3	2.3007	***3-2-3***	**4.6013**
3-1-4	1.2549	*3-2-4*	2.5098
3-3-1	2.1961	*3-4-1*	1.2549
3-3-2	4.3922	*3-4-2*	2.5098
3-3-3	**7.3203**	***3-4-3***	**4.6013**

3-3-4	4.3922	*3-4-4*	2.0915
4-1-1	0.2092	*4-2-1*	0.6275
4-1-2	0.6275	*4-2-2*	1.0458
4-1-3	1.2549	*4-2-3*	2.5098
4-1-4	0.5229	*4-2-4*	1.0458
4-3-1	1.2549	*4-4-1*	0.4706
4-3-2	2.5098	*4-4-2*	0.9412
4-3-3	**4.6013**	*4-4-3*	1.8824
4-3-4	2.0915	*4-4-4*	0.6275

D. References

1. J. Neugebauer and B. A. Hess, *The Journal of Chemical Physics*, 2003, **118**, 7215-7225.
2. M. Supur, S. R. Smith and R. L. McCreery, *Anal. Chem.*, 2017, **89**, 6463-6471.